

~~CONFIDENTIAL~~

NASA MEMO 10-1-58H



1.   
 2.   
 3.   
 4.   
 5.   
 6.   
 7.   
 8.   
 9.   
 10.   
 11.   
 12.   
 13.   
 14.   
 15.   
 16.   
 17.   
 18.   
 19.   
 20.   
 21.   
 22.   
 23.   
 24.   
 25.   
 26.   
 27.   
 28.   
 29.   
 30.   
 31.   
 32.   
 33.   
 34.   
 35.   
 36.   
 37.   
 38.   
 39.   
 40.   
 41.   
 42.   
 43.   
 44.   
 45.   
 46.   
 47.   
 48.   
 49.   
 50.   
 51.   
 52.   
 53.   
 54.   
 55.   
 56.   
 57.   
 58.   
 59.   
 60.   
 61.   
 62.   
 63.   
 64.   
 65.   
 66.   
 67.   
 68.   
 69.   
 70.   
 71.   
 72.   
 73.   
 74.   
 75.   
 76.   
 77.   
 78.   
 79.   
 80.   
 81.   
 82.   
 83.   
 84.   
 85.   
 86.   
 87.   
 88.   
 89.   
 90.   
 91.   
 92.   
 93.   
 94.   
 95.   
 96.   
 97.   
 98.   
 99.   
 100.

553975  
36P

Classification changed to declassify  
effective 1 April 1968 under  
authority of NASA OJN 2 by  
J. J. Carroll. *VC*

NASA MEMO 10-1-58H

13885

# NASA

## MEMORANDUM

LIFT AND DRAG OF A SWEEP-WING FIGHTER AIRPLANE  
AT TRANSONIC AND SUPERSONIC SPEEDS

By Jack Nugent

High-Speed Flight Station  
Edwards, Calif.

### CASE FILE COPY

This material contains information in the meaning of the espionage laws, Title 18, U.S.C., Secs. 793 and 794, the transmission or revelation of which in any manner to an unauthorized person is prohibited by law.

# NATIONAL AERONAUTICS AND SPACE ADMINISTRATION

WASHINGTON  
January 1959

CONFIDENTIAL

NATIONAL AERONAUTICS AND SPACE ADMINISTRATION

MEMORANDUM 10-1-58H

LIFT AND DRAG OF A SWEEP-WING FIGHTER AIRPLANE

AT TRANSONIC AND SUPERSONIC SPEEDS\*

By Jack Nugent

SUMMARY

A flight investigation was made of the lift and drag of a swept-wing fighter airplane in the basic configuration and in a slats-locked-closed configuration over a Mach number range from about 0.63 to about 1.44.

At a nominal lift coefficient of 0.1 negligible drag-coefficient difference existed between the two configurations over a comparable Mach number and altitude range. For the basic configuration at zero lift the supersonic drag level was about three times as great as the subsonic drag level, which was about 0.01, whereas the drag-due-to-lift factor increased about 137 percent over the test Mach number range. At comparable Mach numbers the high-altitude data produced a larger lift-curve slope and showed a more pronounced variation of lift-curve slope in the transonic region than did the low-altitude data. For the high-altitude data the lift-curve slope at a Mach number of 1.44 was approximately 62 percent of the value at a Mach number of 0.9.

INTRODUCTION

In recent years the NASA High-Speed Flight Station, Edwards, Calif., has conducted in-flight lift and drag measurements on current airplanes as part of the joint Air Force-Navy-NASA high-speed flight research program. This paper presents the results of flight tests of a swept-wing fighter airplane with speed capabilities varying from subsonic to well within the supersonic region. Lift and drag measured for the basic configuration (free-floating wing leading-edge slats) are presented. The Mach number range extended from about 0.63 to about 1.44 over the usable lift range of the airplane. Data were obtained over an altitude range from about 20,000 to about 40,000 feet during push-down turn maneuvers and

\*Title, Unclassified.

Restriction/Classification  
Cancelled

CONFIL

accelerated maneuvers; limited data were obtained from speed runs. Data for a configuration in which the slats were locked closed for all flight conditions also were obtained concurrently with a maneuvering-characteristics program. The Mach number range of these tests extended from about 0.87 to about 1.13 over the usable lift range of the airplane.

#### SYMBOLS

$A$	aspect ratio, or cross-sectional area, sq ft
$A_d$	inlet duct area at pressure-measuring station, sq ft
$A_e$	exit area of jet nozzle measured cold, sq ft
$a_n$	measured normal acceleration, g units
$a_x$	measured longitudinal acceleration, g units
$C_D$	airplane aerodynamic drag coefficient
$\frac{dC_D}{dC_L^2}$	drag-due-to-lift factor
$\Delta C_D = C_{D_b} - C_{D_s}$	
$C_f$	turbojet nozzle coefficient
$C_L$	airplane aerodynamic lift coefficient
$C_{L_\alpha}$	slope of lift curve, $\text{deg}^{-1}$ , $\text{radians}^{-1}$
$c$	wing chord, ft
$\bar{c}$	wing mean aerodynamic chord, ft
$F_j$	gross thrust, lb
$F_n$	net thrust, $F_j - F_r$ , lb

$F_r$	ram drag, lb
$g$	acceleration due to gravity, ft/sec <sup>2</sup>
$h_p$	pressure altitude, ft
$k_1$	local slope of engine thrust-rotational speed curve, lb/rpm
$k_2$	constant for flight at a given Mach number, $k_1 \frac{\delta_c}{p_a}$ , sq ft/rpm
$l$	configuration length, ft
$(L/D)_{max}$	maximum value of lift-drag ratio
$M$	airplane Mach number
$M_d$	inlet-duct Mach number at pressure-measuring station
$N_l$	low-speed rotor, revolutions per minute
$p_a$	ambient static pressure, lb/sq ft
$p_d$	inlet-duct static pressure at pressure-measuring station, lb/sq ft
$p'$	total pressure at compressor face, lb/sq ft
$p'_e$	total pressure near jet-nozzle exit, lb/sq ft
$q$	free-stream dynamic pressure, $0.7M^2 p_a$ , lb/sq ft
$S$	wing area, sq ft
$T_t$	total temperature at compressor face (assumed equal to free stream), °R
$W$	airplane weight, lb
$\alpha$	angle of attack of airplane center line, deg
$\delta_c$	ratio of compressor-face pressure to standard NACA sea-level pressure, $\frac{p'}{2116}$

- $\epsilon$  angle between airplane thrust axis and airplane center line, deg
- $\theta_c$  ratio of compressor-face temperature to NACA sea-level standard,  $T_t$  518.4

Subscripts:

- b basic configuration
- s slats-locked-closed configuration

### AIRPLANE AND PROPULSION SYSTEM

The test airplane is a swept-wing fighter airplane capable of supersonic speeds. The 25-percent-wing chord line is swept back  $45^\circ$ , and the fuselage is characterized by a relatively flat bottom and positive camber. Figure 1 presents a photograph of the test airplane, and figure 2 is a three-view drawing. Longitudinal control is effected by means of an all-movable stabilizer placed beneath the extended wing chord plane. Each wing leading edge is equipped with an extensible slat consisting of five separate constant-chord sections and extending from about 25-percent to about 95-percent semispan. The slat is automatic in operation and opens as a function of local wing loading (ref. 1). Additional physical characteristics of the airplane are given in table I. Figure 3 presents the normal cross-sectional-area distribution in nondimensional form.

The propulsion system incorporates a sharp-lipped normal-shock nose inlet. The power plant is the J57 dual rotor turbojet engine with afterburner and a two-position iris-type nozzle. The bare engine military and afterburner thrusts are about 9,000 and 15,000 pounds, respectively, at static sea-level conditions.

### INSTRUMENTATION

Standard NASA recording instruments were installed in the airplane to measure the following pertinent quantities:

Airspeed  
Altitude  
Normal and longitudinal acceleration  
Angle of attack

Inlet-duct static and total pressure  
 Jet-nozzle-exit total pressure  
 Slat position  
 Engine revolutions per minute, high speed and low speed  
 Free-stream total temperature  
 Stabilizer position

All instruments were synchronized by a common timer.

Altitude and airspeed were determined by an NACA airspeed tube mounted on the nose boom, and angle of attack was measured by a vane attached to an arm projecting from the nose boom (airplane E of ref. 2). The vane was approximately 56.4 inches ahead of the inlet and 7 inches to the left of the center line of the boom.

#### THRUST AND DRAG DETERMINATION

Gross thrust was determined in flight by measuring exit-nozzle total pressure and free-stream static pressure. Exit-nozzle total pressure was measured with an air-cooled cantilever-type probe inserted into the gas stream approximately in the jet-nozzle-exit plane. For most of the tests reported in this paper sonic flow was established at the jet-nozzle exit, permitting use of the following equation for gross thrust for both afterburning and nonafterburning operation

$$F_j = C_f A_e (1.254 p'_e - p_a)$$

The value of  $C_f$  was determined from ground runs on a thrust stand and was essentially the same for afterburning and nonafterburning operation. Because  $C_f$  varies with exhaust-pressure ratio and because higher pressure ratios are attained in flight than on the ground, it was necessary to extrapolate the ground data to the higher pressure ratios. The extrapolation was made in conformance with trends shown by altitude-chamber tests. Figure 4 presents a typical thrust-stand calibration.

Duct total pressure was measured with three vertical rakes of four manifolded probes per rake each placed in the plane of the survey station which was near the inlet. The three rakes were connected to yield one total pressure. Static pressure was measured with two connected wall static taps.

Ram drag was determined from the following equation:

$$F_r = 1.4 p_d A_d M M_d \sqrt{\frac{1 + 0.2 M_d^2}{1 + 0.2 M^2}}$$

Local Mach number in the duct was determined from measurements of total and static pressure.

The derivation and limitations of the foregoing equations are discussed in reference 3.

Following are the basic equations for the computation of the lift and drag coefficients:

$$C_L = \frac{W}{qS} (a_n \cos \alpha + a_x \sin \alpha) - \frac{F_j}{qS} \sin (\epsilon + \alpha) \quad (1)$$

$$C_D = \frac{W}{qS} (a_n \sin \alpha - a_x \cos \alpha) + \frac{F_j}{qS} \cos (\epsilon + \alpha) - \frac{F_r}{qS} \quad (2)$$

#### TESTS

Lift and drag were measured for both afterburning and nonafterburning operation. Most of the data at Mach numbers greater than about 0.95 were obtained with the afterburner on, regardless of altitude.

The first series of tests was performed with the leading-edge slats operating in the normal manner. A Mach number range from about 0.63 to about 1.44 was covered. For Mach numbers below about 1.1 the data were obtained at altitudes of about 20,000 feet, whereas the data above about 1.1 were obtained at altitudes greater than 20,000 feet and largely at 40,000 feet. The tests consisted of push-down turn maneuvers (ref. 4) and speed runs.

The second test series was performed at altitudes from about 35,000 to about 40,000 feet covering a Mach number range from about 0.87 to 1.13. For these tests the various slat segments were fastened to the wing so that no slat movement was possible under any flight conditions. The tests consisted of wind-up turns.

The final test series was instigated as a check on the results of the first two test series and was obtained at a later date after the thrust instrumentation had been removed. Therefore, it was possible

only to measure thrust-minus-drag of the airplane. Two flights were made at altitudes of 20,000 and 30,000 feet with the slats free-floating and sealed. The second flight was performed immediately after the first so that the ambient conditions at altitude were approximately equal. The flights consisted of level-flight accelerations until the pilot felt that terminal Mach number was reached.

The test Reynolds number varied from about 25 million to about 48 million, based on the wing mean aerodynamic chord. Stabilizer position varied from 0° to about 18°, airplane nose-up.

ANALYSIS OF THE FINAL TEST SERIES

Since the final tests were obtained some time after the initial tests, and since the thrust instrumentation had been removed from the airplane, it was possible to measure only thrust-minus-drag of the airplane. However, the following analysis permits an estimate of any drag difference for the two configurations. For the speed runs employed in the final test, by assuming that the angles  $\alpha$  and  $\epsilon$  are essentially 0, equation (2) can be simplified as follows:

$$C_{D_b} = \frac{1}{q_b S} \left[ (F_j - F_r)_b - W a_{x_b} \right]$$

and

$$C_{D_s} = \frac{1}{q_s S} \left[ (F_j - F_r)_s - W a_{x_s} \right]$$

Assuming

$$F_j - F_r = F_n$$

Then

$$\Delta C_D = C_{D_b} - C_{D_s} = \frac{1}{0.7 M^2 S} \left[ \frac{F_{n_b}}{p_{a_b}} - \frac{F_{n_s}}{p_{a_s}} - \left( \frac{W a_{x_b}}{p_{a_b}} - \frac{W a_{x_s}}{p_{a_s}} \right) \right]$$

At a given Mach number and duct efficiency the engine net thrust can be expressed as a function of the corrected engine speed, since Reynolds number and angle-of-attack effects are negligible.

$$\Delta C_D = \frac{1}{0.7M^2S} \left[ \left( \frac{F_n}{\delta_{c_b}} \right) \frac{\delta_{c_b}}{p_{a_b}} - \left( \frac{F_n}{\delta_{c_s}} \right) \frac{\delta_{c_s}}{p_{a_s}} \right] - \frac{1}{0.7M^2S} \left[ \left( \frac{W_{a_x_b}}{p_{a_b}} - \frac{W_{a_x_s}}{p_{a_s}} \right) \right]$$

$$\Delta C_D = \frac{k_1}{0.7M^2S} \left[ \left( \frac{N_1}{\sqrt{\theta_c}} \right) \frac{\delta_{c_b}}{p_{a_b}} - \left( \frac{N_1}{\sqrt{\theta_c}} \right) \frac{\delta_{c_s}}{p_{a_s}} \right] - \frac{1}{0.7M^2S} \left[ \left( \frac{W_{a_x_b}}{p_{a_b}} - \frac{W_{a_x_s}}{p_{a_s}} \right) \right]$$

$$= \frac{k_2}{0.7M^2S} \left[ \left( \frac{N_1}{\sqrt{\theta_c}} \right)_b - \left( \frac{N_1}{\sqrt{\theta_c}} \right)_s \right] - \frac{1}{0.7M^2S} \left[ \left( \frac{W_{a_x_b}}{p_{a_b}} - \frac{W_{a_x_s}}{p_{a_s}} \right) \right]$$

$$\Delta C_D = \frac{k_2}{0.7M^2S} \left[ \Delta \frac{N_1}{\sqrt{\theta_c}} \right] - \frac{1}{0.7M^2S} \left[ \left( \frac{W_{a_x_b}}{p_{a_b}} - \frac{W_{a_x_s}}{p_{a_s}} \right) \right] \quad (3)$$

Therefore, a plot of the right-hand side of equation (3) against Mach number gives a direct indication of any drag difference between the two configurations for the speed runs.

#### ACCURACY

The following accuracies are applicable for the results presented:

$\alpha$ , deg . . . . .	$\pm 0.5$ (average)
$a_n$ , g . . . . .	$\pm 0.05$
$a_x$ , g . . . . .	$\pm 0.0025$
$F_j$ , lb . . . . .	150
$F_r$ , lb . . . . .	100
M . . . . .	$\pm 0.01$ subsonically, supersonically $\pm 0.02$ transonically
q (at M = 0.8 and $h_p = 37,500$ ft), lb/sq ft . . . . .	$\pm 5$
W, lb . . . . .	$\pm 100$

A detailed discussion of the sources contributing to errors in measurement of these quantities is given in references 2 and 3.

The error in lift coefficient is 5 percent or less throughout the lift range presented. The accuracy of the drag coefficient depends

primarily on the accuracies of thrust, angle of attack, longitudinal acceleration, normal acceleration, weight, and Mach number. It is believed that the faired values of drag coefficient are accurate within  $\pm 0.001$  at low lift and higher values of dynamic pressure.

## RESULTS AND DISCUSSION

Figures 5 and 6 present lift coefficient plotted against angle of attack for the basic configuration and the slats-locked-closed configuration, respectively, for several Mach numbers; the data were obtained from the first and second test series. The Mach number variation for each plot was kept low; in the drag-rise region the variation was  $\pm 0.01$  and elsewhere was  $\pm 0.02$ . Some nonlinearities are present in the curves; the nonlinearities at zero lift are due, possibly, to fuselage contribution as a result of camber. For the slats-locked-closed configuration (fig. 6) the data are generally insufficient to determine any nonlinearities at low lift.

Figure 7 compares the lift data of figures 5 and 6 at three selected Mach numbers. It will be noted that there are differences in the lift curves below the lift coefficient at which the slats start to open; the difference must either be the effect of the altitude change between the two sets of data, the result of some minor condition such as slat leakage, or the precision of measurement. During the final test series mentioned previously, the airplane was flown at a constant altitude with the slats free floating and locked closed and sealed; these tests showed conclusively that the effect was not the result of slat movement or leakage. However, in these tests only overall lift measurements were made, so the exact manner in which the lift is affected by altitude is not explained. (The airplane manufacturer's estimated data indicate changes in lift-curve slope due to structural flexibility equal to about one-half of those shown by these tests.) It should be noted that at a lift coefficient of about 0.3, about  $0.5^\circ$  more angle of attack is required to produce a given lift coefficient at the low-altitude conditions than at the high-altitude conditions. Although the overall accuracy of measurement of angle of attack was only  $0.5^\circ$ , it is believed that comparative measurements with the same system have a higher accuracy and hence the differences shown are real.

The slopes of the lift curves of figures 5 and 6 are plotted against Mach number in figure 8. Slopes were obtained for lift coefficients corresponding closely to 1 g flight for the test altitude and at a nominal weight of 22,000 pounds. At comparable Mach numbers the high-altitude data produced a higher lift-curve slope, with a maximum difference occurring at a Mach number of about 0.92, corresponding to a

peak  $C_{L\alpha}$  of 0.068 for the high-altitude data. In addition, the high-altitude data show a more pronounced variation in the transonic region. For the high-altitude data the lift-curve slope at a Mach number of 1.44 was approximately 62 percent of the value at a Mach number of 0.9.

Figure 9 presents drag coefficient plotted against lift coefficient for the basic configuration at altitudes of 20,000 and 40,000 feet. The lift-coefficient and Mach number variation corresponds to the data of figure 5. The drag-coefficient data corresponding to the lift curves of figure 6 are not presented. The data were obtained at too low values of  $q$ , which produced larger errors in drag coefficient (i.e., for a given error in thrust,  $\alpha$ , etc.) than were encountered in the lower altitude data and rendered presentation unsuitable.

The drag data from the final test series are presented in figure 10 as the drag-coefficient difference between the basic and slats-locked-closed configurations plotted as a function of Mach number at a given altitude. The analysis is given in the ANALYSIS OF THE FINAL TEST SERIES section. The data indicate essentially negligible drag difference between the two configurations at altitudes of 20,000 and 30,000 feet for the test speeds; in addition, there was no difference between the terminal Mach numbers reached for the two configurations. The test lift coefficient was nominally 0.1 for both altitudes.

Figure 11 shows the data of figure 9 plotted against Mach number for lift coefficients of 0 and 0.2. In the subsonic region the drag-coefficient levels remain relatively constant; in the supersonic region the drag-coefficient levels increase for Mach numbers greater than about 1.25. The drag-rise Mach number, taken as that corresponding to  $\frac{dC_D}{dM} = 0.1$ , was about 0.94 for both curves. At zero lift the supersonic drag-coefficient level was about three times as great as the subsonic drag level, which was about 0.01. Wind-tunnel data from reference 5 are presented for comparison. The data of reference 5 have been extrapolated to the flight test value of Reynolds number using theoretical turbulent skin friction data. It should also be mentioned that geometric differences existed between the scale-model data of reference 5 and the full-scale airplane, notably in the tail thicknesses. In addition, the model had no simulation of internal flow. Considering these differences, it is believed that reasonable agreement is shown between the two sets of data.

Figure 12 presents the variation of  $(L/D)_{\max}$  and  $C_L$  for  $(L/D)_{\max}$  with Mach number for the data of figure 9. The value of  $C_L$  for  $(L/D)_{\max}$  is confined between values of 0.25 and 0.35 for the test

range; the supersonic value of  $(L/D)_{\max}$  was about 35 percent of the subsonic value.

Figure 13 presents the data of figures 5 and 9 plotted as  $C_D$  against  $C_L^2$ . Straight-line fairings were made for lift-coefficient-squared values less than about 0.16. The slopes of the straight lines so obtained are a measure of the drag due to lift. Figure 14 presents the variation of drag-due-to-lift factor with Mach number; the value increases through the Mach number range to a supersonic value about 137 percent the subsonic value. Altitude effects are assumed negligible. The values of  $dC_D/dC_L^2$  corresponding to zero  $(1/C_{L\alpha})$  and full leading-edge suction  $(1/\pi A)$  for low and high altitudes are also presented; these data indicate a decrease in leading-edge suction as speeds are increased above subsonic values.

### CONCLUSIONS

Flight tests of the lift and drag of a swept-wing fighter airplane in the basic configuration and in the slats-locked-closed configuration for a Mach number range from 0.63 to 1.44 and altitudes of 20,000 feet to 40,000 feet led to the following conclusions:

1. At a nominal lift coefficient of 0.1 negligible drag-coefficient difference existed between the two configurations over a comparable Mach number and altitude range.
2. For the basic configuration at zero lift the supersonic drag level was about three times as great as the subsonic drag level, which was about 0.01, whereas the drag-due-to-lift factor increased about 137 percent over the test Mach number range.
3. At comparable Mach numbers the high-altitude data produced a larger lift-curve slope and showed a more pronounced variation of lift-curve slope in the transonic region than did the low-altitude data.
4. For the high-altitude data the lift-curve slope at a Mach number of 1.44 was approximately 62 percent of the value at a Mach number of 0.9.

High-Speed Flight Station,  
National Aeronautics and Space Administration,  
Edwards, Calif., July 3, 1958.

## REFERENCES

1. Arabian, Donald D., Runckel, Jack F., and Reid, Charles F., Jr.: Aerodynamic Load Measurements and Opening Characteristics of Automatic Leading-Edge Slats on a  $45^{\circ}$  Sweptback Wing at Transonic Speeds. NACA RM L53I30, 1954.
2. Larson, Terry J., Stillwell, Wendell H., and Armistead, Katharine H.: Static-Pressure Error Calibrations for Nose-Boom Airspeed Installations of 17 Airplanes. NACA RM H57A02, 1957.
3. Beeler, De E., Bellman, Donald R., and Saltzman, Edwin J.: Flight Techniques for Determining Airplane Drag at High Mach Numbers. NACA TN 3821, 1956.
4. Matranga, Gene J., and Armistead, Katharine H.: Flight Evaluation of the Effects of Leading-Edge-Slat Span on the Stability and Control Characteristics of a Swept-Wing Fighter-Type Airplane During Accelerated Longitudinal Maneuvers at Transonic Speeds. NACA RM H58A03a, 1958.
5. Whitcomb, Charles F., and Lee, Edwin E., Jr.: Drag Investigation of a Swept-Wing Fighter-Airplane Model Incorporating Two Drag-Rise-Reducing Fuselage Revisions. NACA RM L55E24, 1955.

TABLE I.- PHYSICAL CHARACTERISTICS OF AIRPLANE

Wing:	
Airfoil section . . . . .	NACA 64A007
Total area (including ailerons and 83.84 sq ft covered by fuselage), sq ft . . . . .	385.21
Span, ft . . . . .	38.58
Mean aerodynamic chord, ft . . . . .	11.16
Root chord, ft . . . . .	15.86
Tip chord, ft . . . . .	4.15
Taper ratio . . . . .	0.262
Aspect ratio . . . . .	3.86
Sweep at 0.25 chord line, deg . . . . .	45
Incidence, deg . . . . .	0
Dihedral, deg . . . . .	0
Geometric twist, deg . . . . .	0
Aileron -	
Area rearward of hinge line (each), sq ft . . . . .	19.32
Span at hinge line (each), ft . . . . .	7.81
Chord rearward of hinge line, percent wing chord . . . . .	25
Travel (each), deg . . . . .	±15
Leading-edge slat -	
Span, equivalent, ft . . . . .	12.71
Segments . . . . .	5
Spanwise location, inboard end, percent wing semispan . . . . .	23.3
Spanwise location, outboard end, percent wing semispan . . . . .	89.2
Ratio of slat chord to wing chord (parallel to fuselage reference line), percent . . . . .	20
Rotation, maximum, deg . . . . .	15
Horizontal tail:	
Airfoil section . . . . .	NACA 65A003.5
Total area (including 31.65 sq ft covered by fuselage), sq ft . . . . .	98.86
Span, ft . . . . .	18.72
Mean aerodynamic chord, ft . . . . .	5.83
Root chord, ft . . . . .	8.14
Tip chord, ft . . . . .	2.46
Taper ratio . . . . .	0.30
Aspect ratio . . . . .	3.54
Sweep at 0.25 chord line, deg . . . . .	45
Dihedral, deg . . . . .	0
Travel, leading edge up, deg . . . . .	5
Travel, leading edge down, deg . . . . .	25
Control system . . . Irreversible hydraulic boost and artificial feel	

TABLE I.- PHYSICAL CHARACTERISTICS OF AIRPLANE - Concluded

Vertical tail:

Airfoil section . . . . .	NACA 65A003.5
Area (excluding dorsal fin and area blanketed by fuselage), sq ft . . . . .	42.7
Area blanketed by fuselage (area between fuselage contour line and line parallel to fuselage reference line through intersections of leading edge of vertical tail and fuselage contour line), sq ft . . . . .	2.45
Span (unblanketed), ft . . . . .	7.93
Mean aerodynamic chord, ft . . . . .	5.90
Root chord, ft . . . . .	8.28
Tip chord, ft . . . . .	2.49
Taper ratio . . . . .	0.301
Aspect ratio . . . . .	1.49
Sweep at 0.25 chord line, deg . . . . .	45
Rudder -	
Area, rearward of hinge line, sq ft . . . . .	6.3
Span at hinge line, ft . . . . .	3.33
Root chord, ft. . . . .	2.27
Tip chord, ft . . . . .	1.50
Travel, deg . . . . .	±20
Spanwise location, inboard end, percent vertical-tail span . . . . .	3.1
Spanwise location, outboard end, percent vertical-tail span . . . . .	44.8
Chord, percent vertical-tail chord . . . . .	28.4
Balance . . . . .	Aerodynamic

Fuselage:

Length (afterburner nozzle closed), ft . . . . .	45.64
Maximum width, ft . . . . .	5.58
Maximum depth over canopy, ft . . . . .	6.37
Side area (total), sq ft . . . . .	230.92
Fineness ratio (afterburner nozzle closed) . . . . .	7.86

Speed brake:

Surface area, sq ft . . . . .	14.14
Maximum deflection, deg . . . . .	50

Power plant:

Turbojet engine . . . . .	One Pratt & Whitney J57 with afterburner
Thrust (guarantee sea level), afterburner, lb . . . . .	15,000
Military, lb . . . . .	9,000

Airplane weight, lb:

Basic (without fuel, oil, water, pilot) . . . . .	20,262
Total (full fuel, oil, water, pilot). . . . .	25,400

Center-of-gravity location, percent  $\bar{c}$ :

Total weight - gear down . . . . .	30.2
Total weight - gear up . . . . .	30.2

CONFIDENTIAL



Figure 1.- Photograph of the test airplane with slats in open position. E-2095

Restriction/Classification  
Cancelled  
CONFIDENTIAL

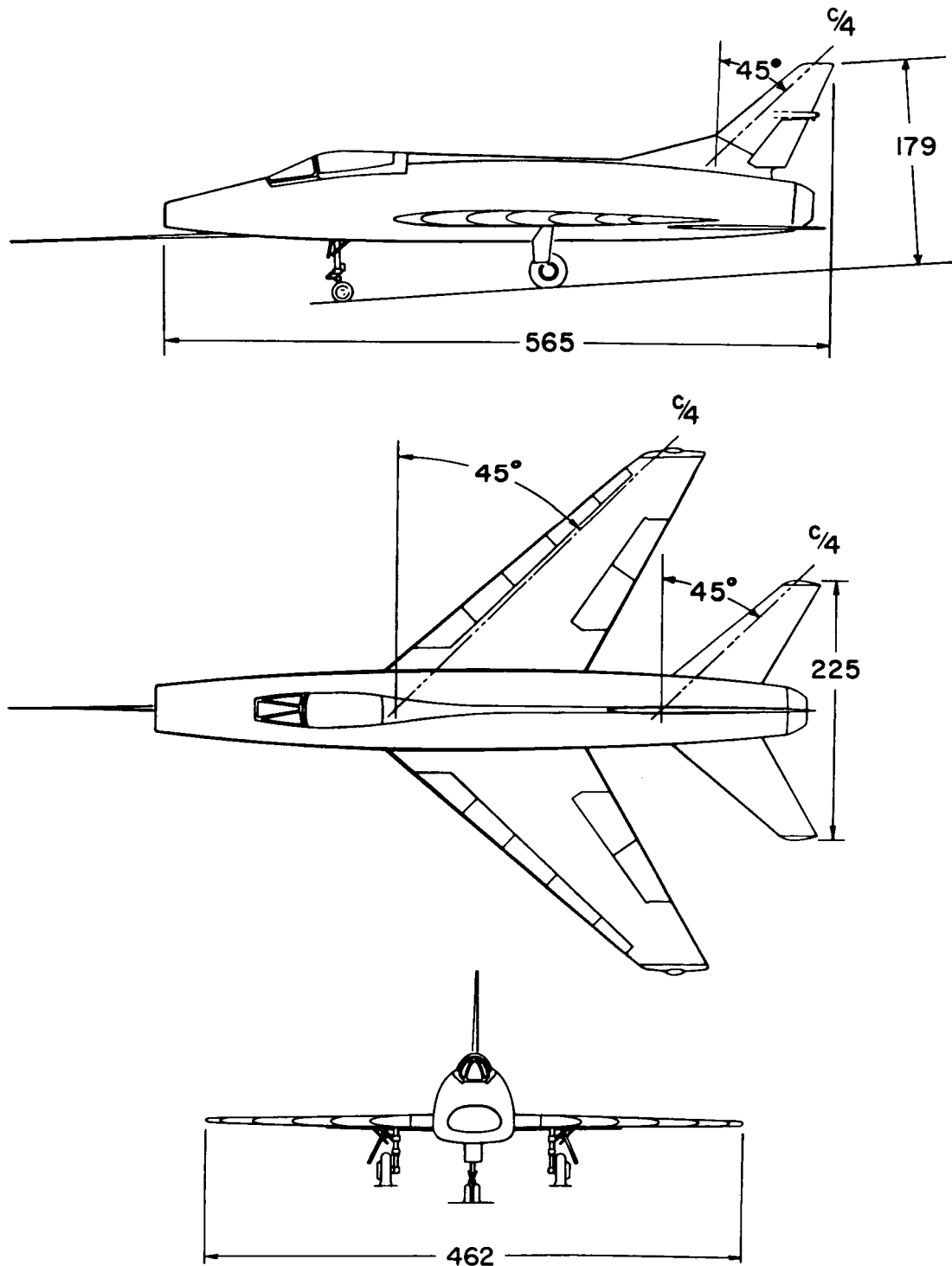


Figure 2.- Three-view drawing of the test airplane. All dimensions in inches.

Restriction/Classification Cancelled

CONFIDENTIAL

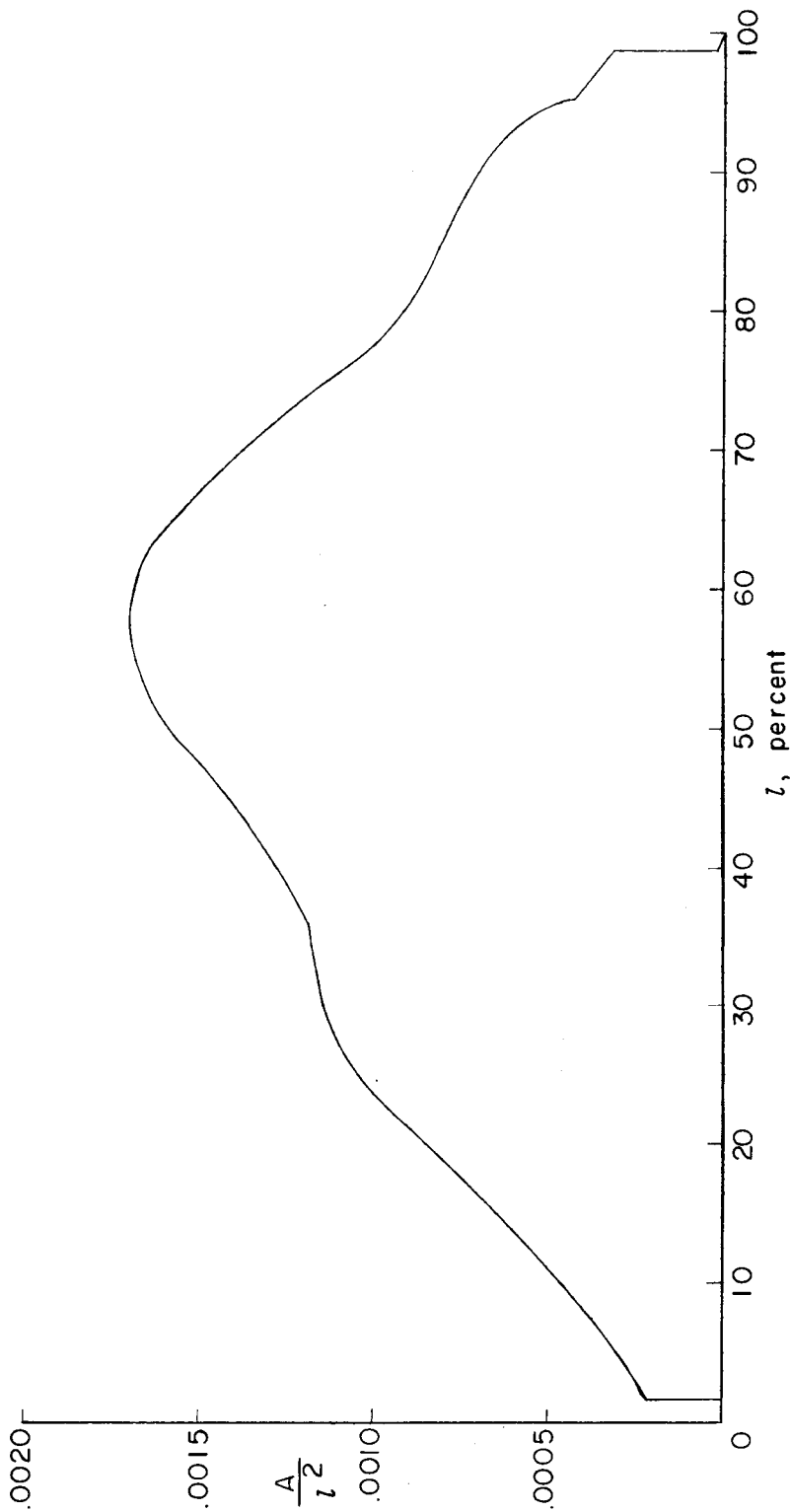


Figure 3.- Normal cross-sectional-area distribution.

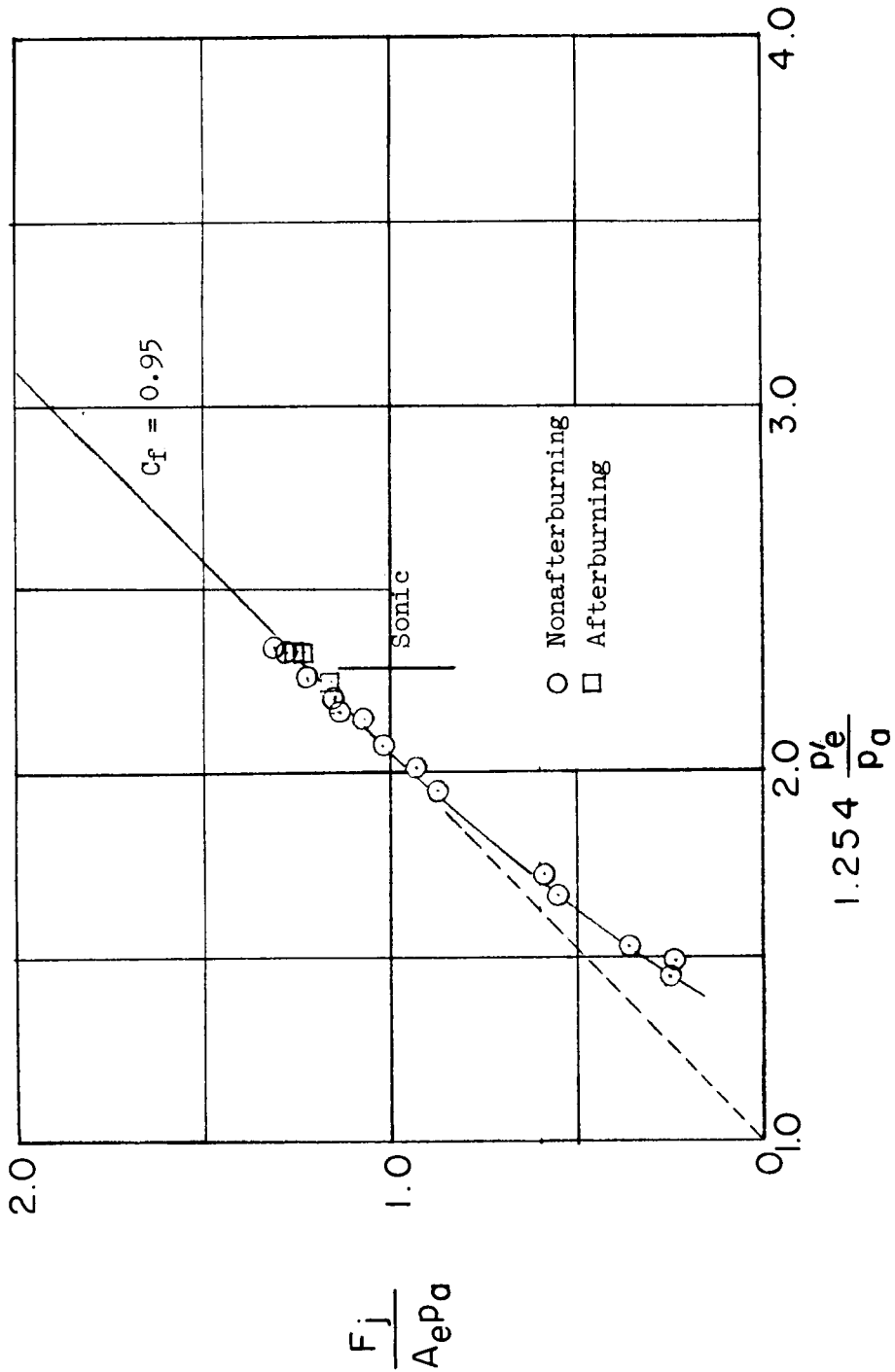


Figure 4.- Typical thrust-stand calibration of exhaust nozzle.

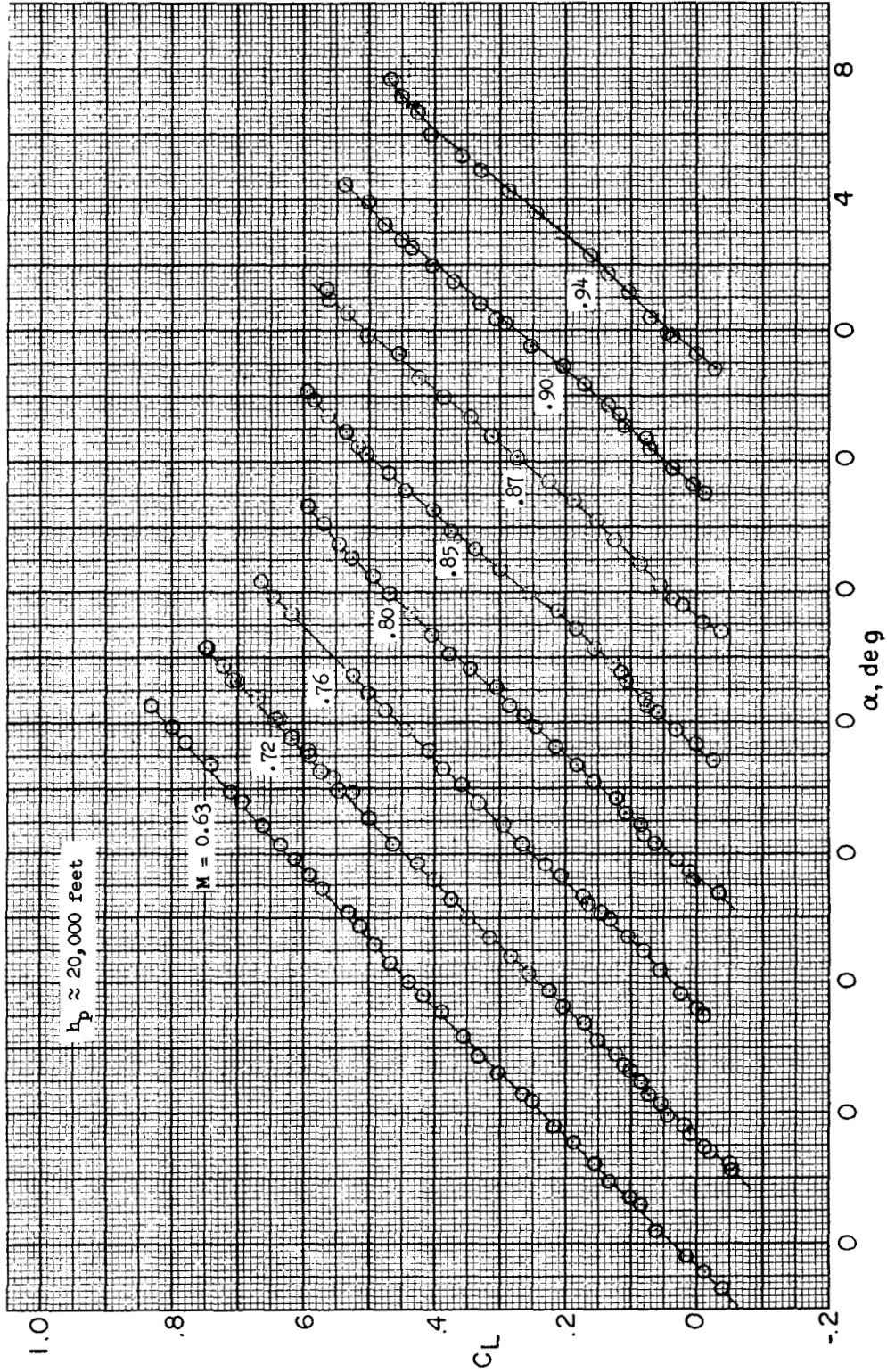


Figure 5.- Variation of  $C_L$  with  $\alpha$  for several Mach numbers. Basic configuration.

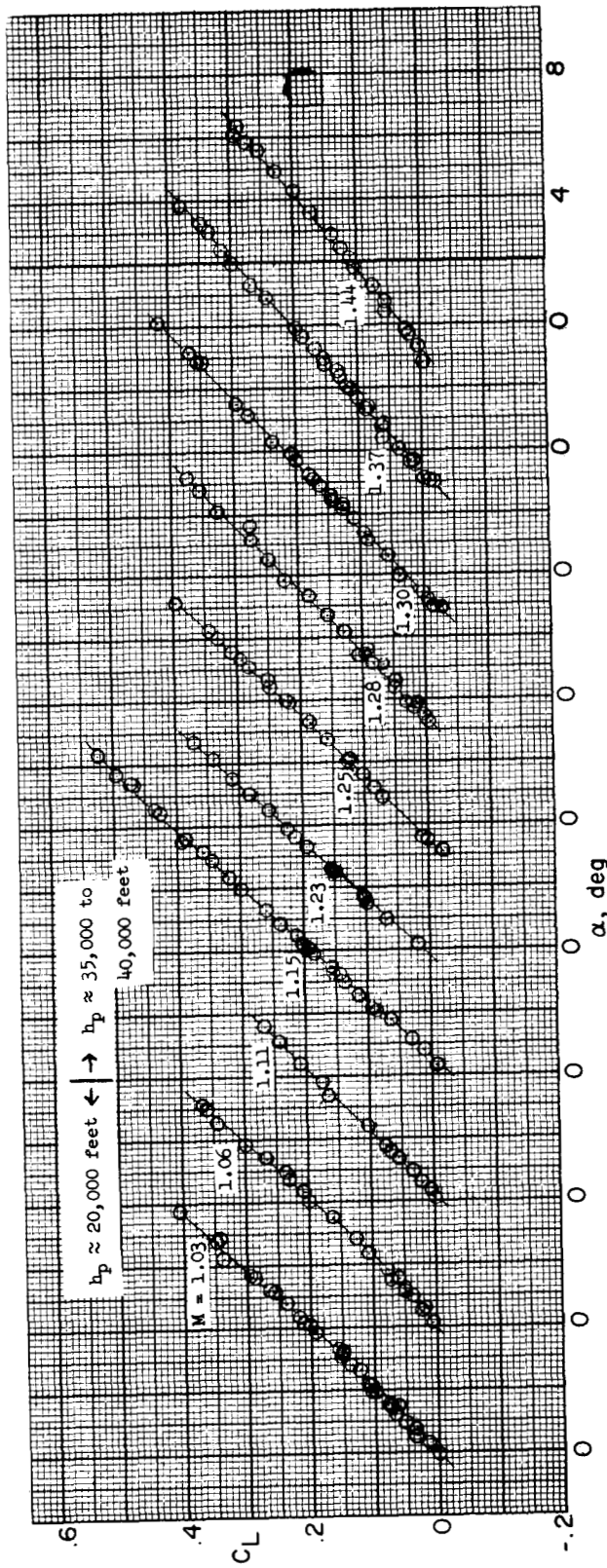


Figure 5.- Concluded.

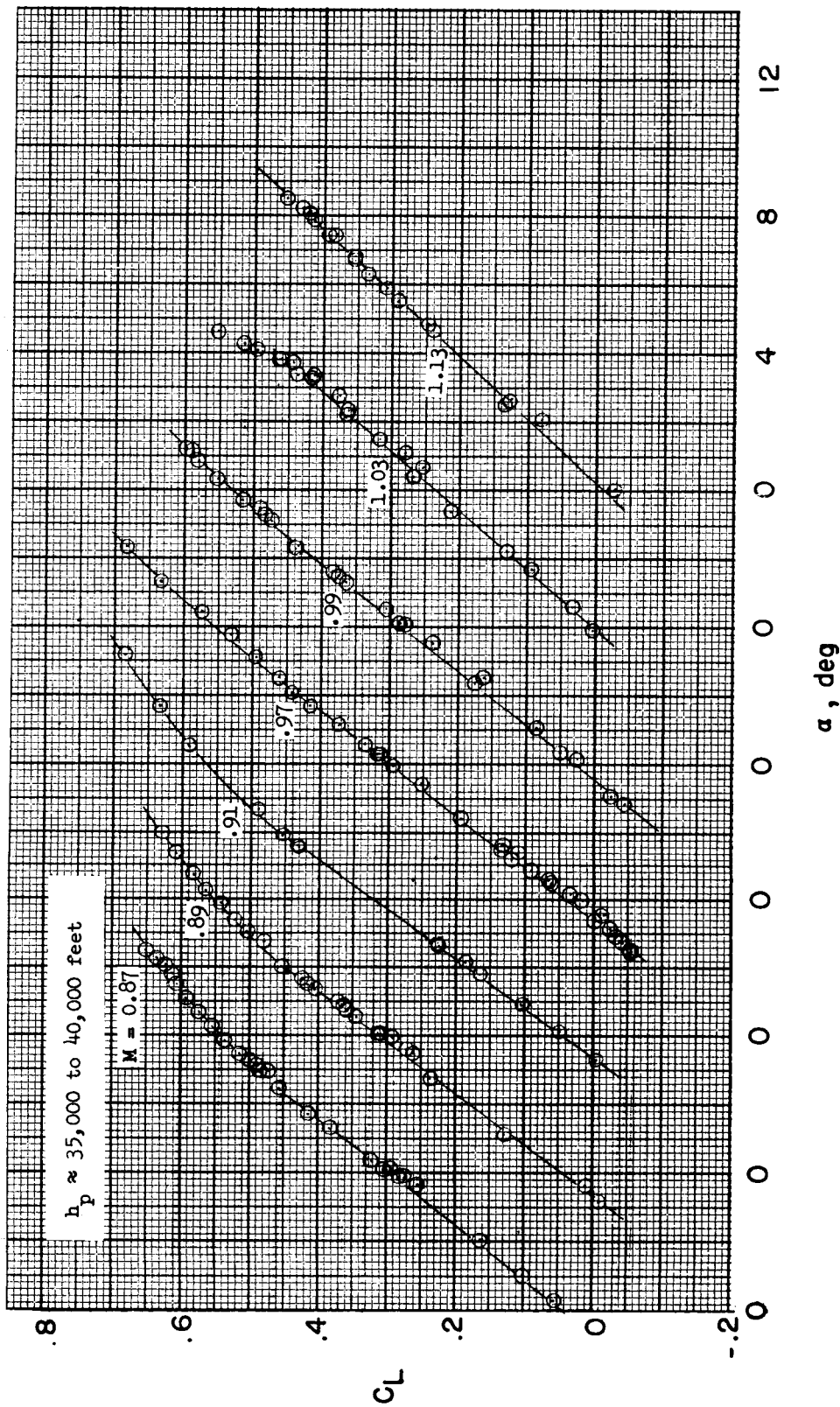


Figure 6.- Variation of  $C_L$  with  $\alpha$  for several Mach numbers. Slats-locked-closed configuration.

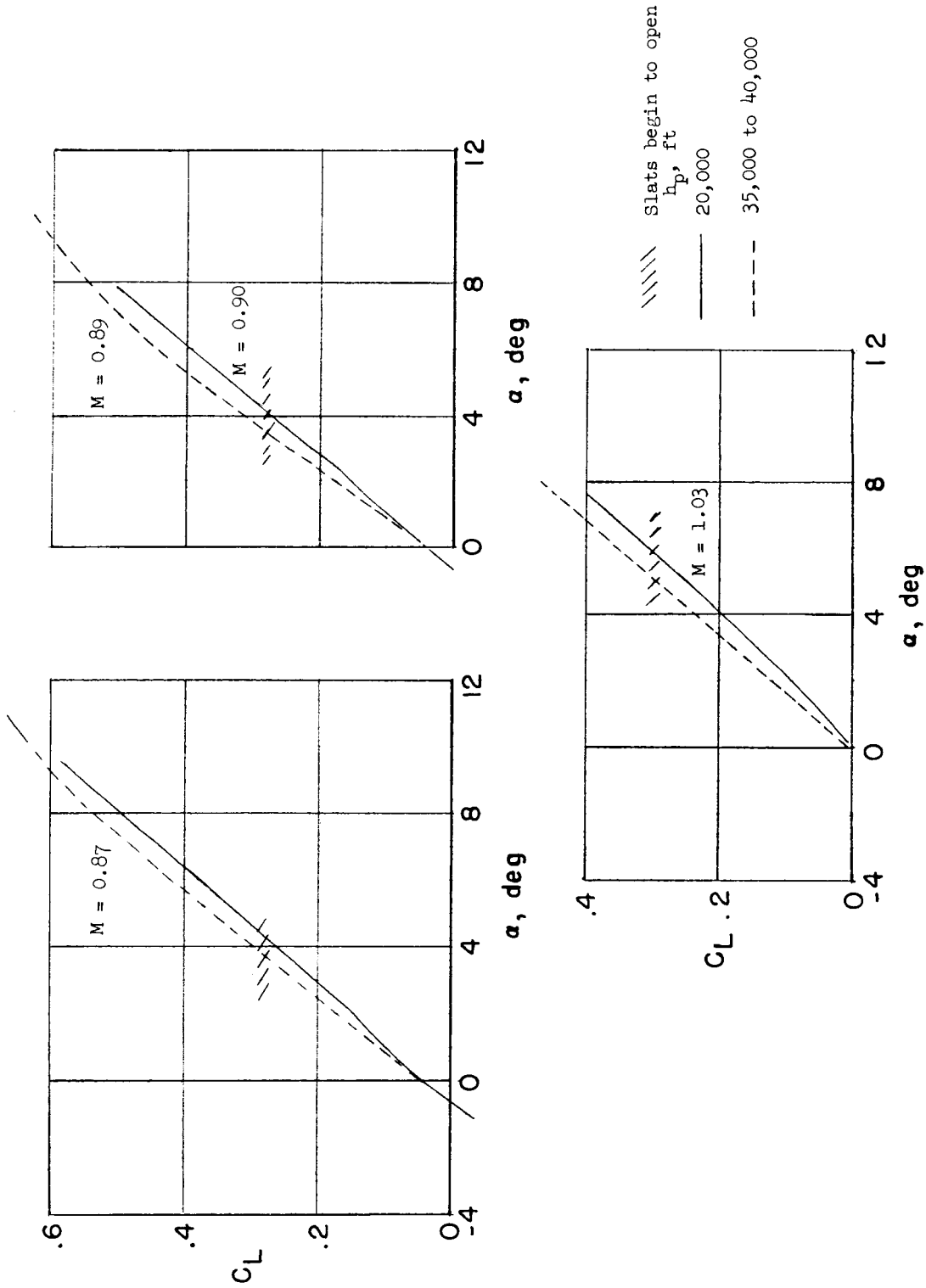


Figure 7.- Effect of altitude on lift curves.

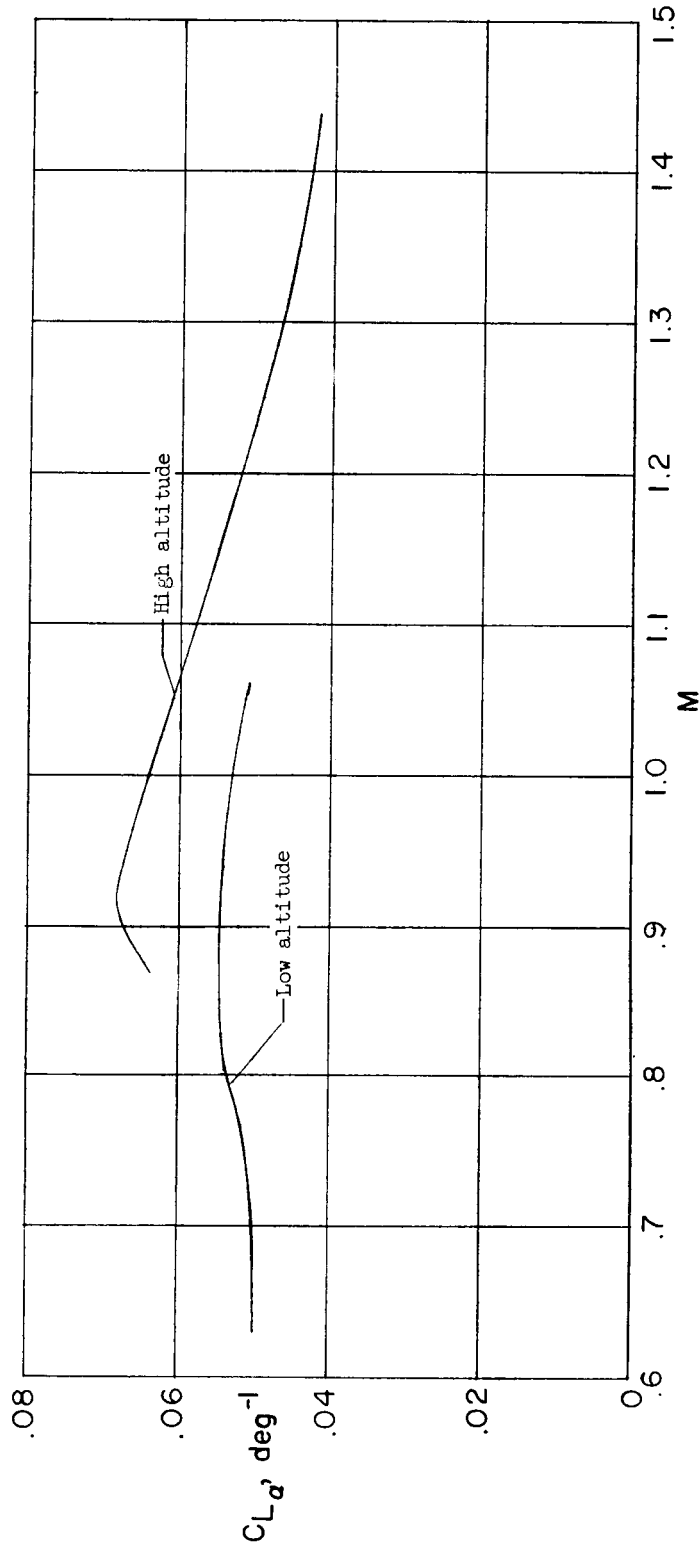


Figure 8.- Comparison of lift-curve slopes for low and high altitudes at 1 g flight.  
W = 22,000 pounds.

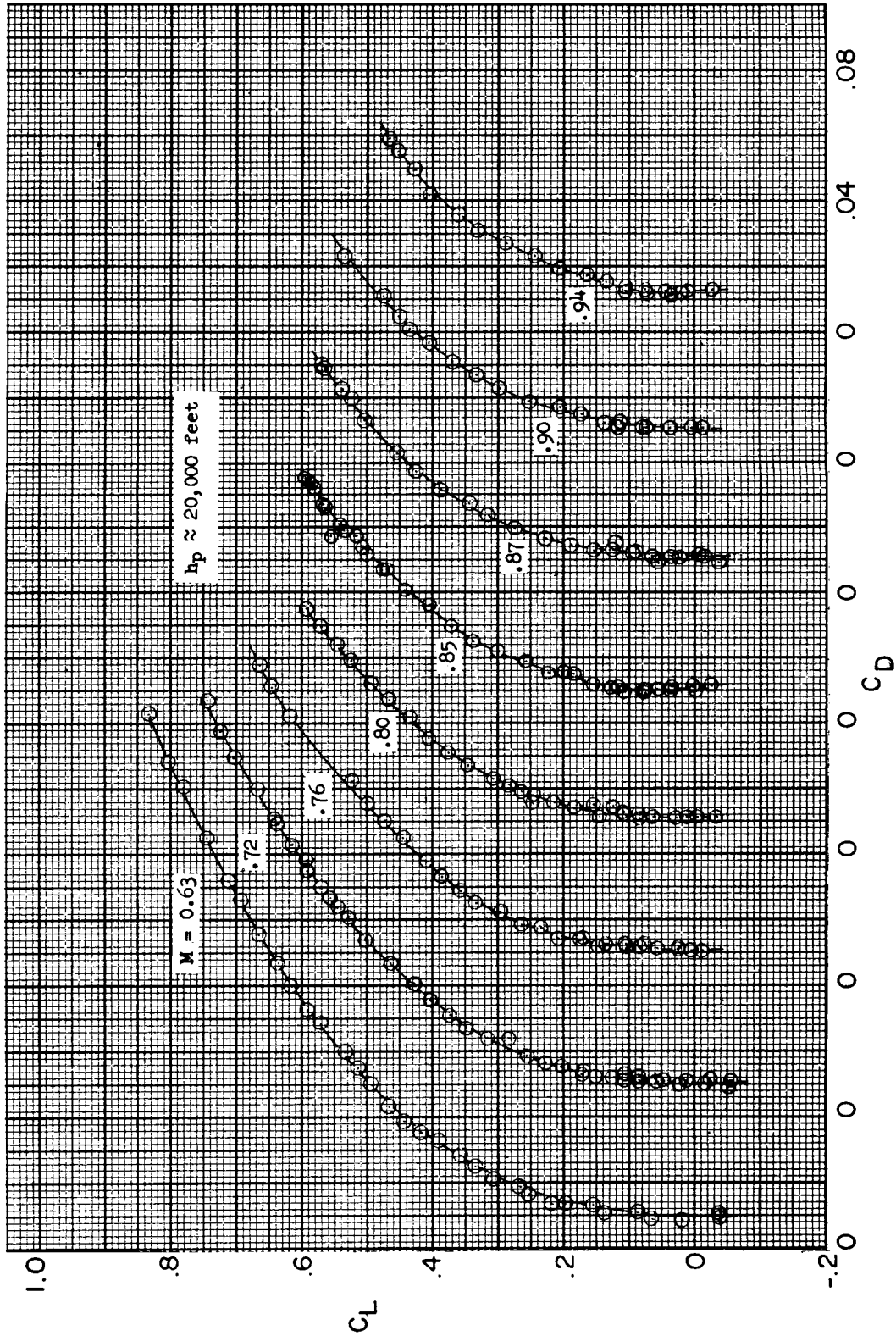


Figure 9.-- Drag coefficient plotted against lift coefficient for several Mach numbers. Basic configuration.

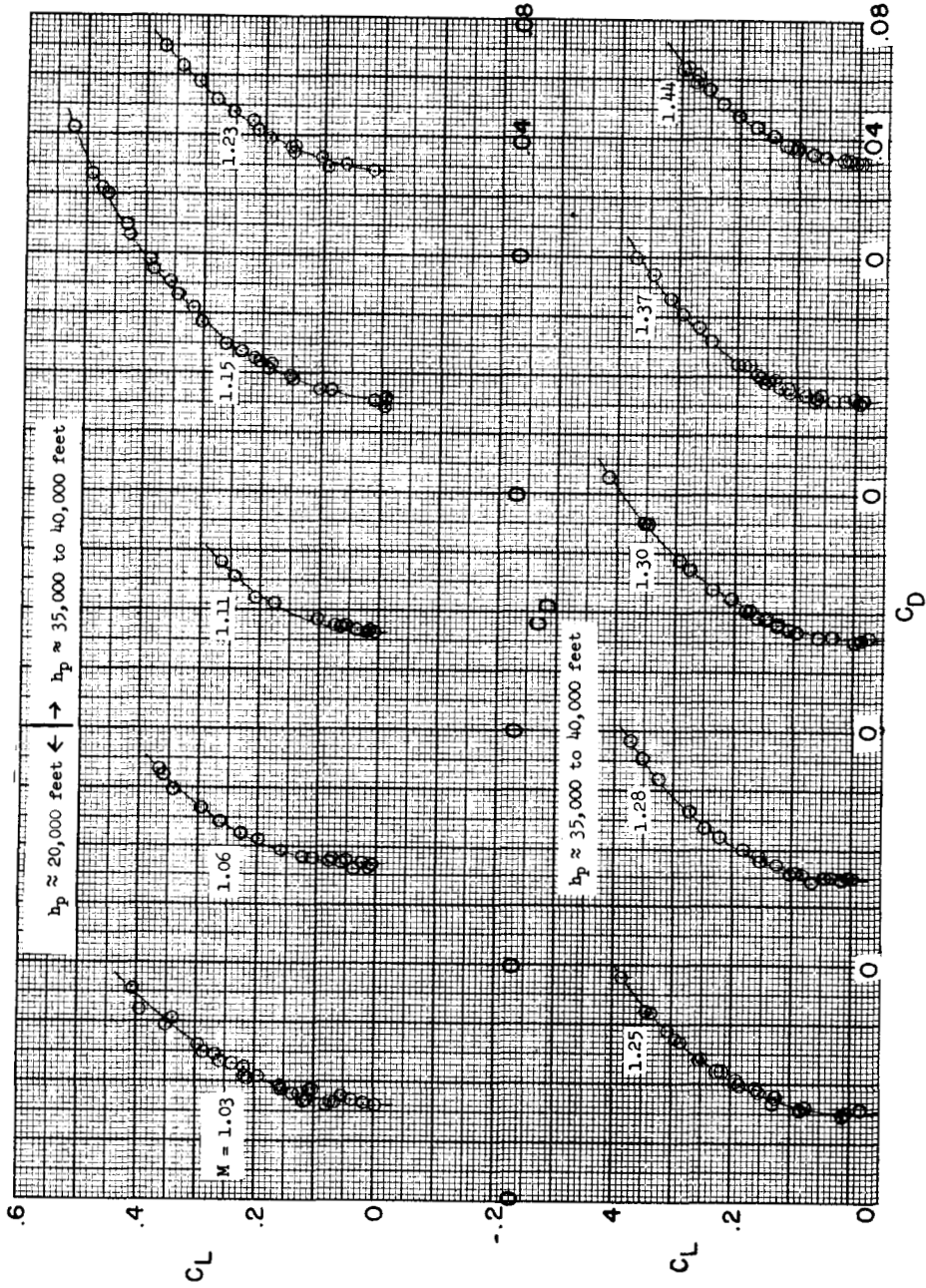


Figure 9.- Concluded.

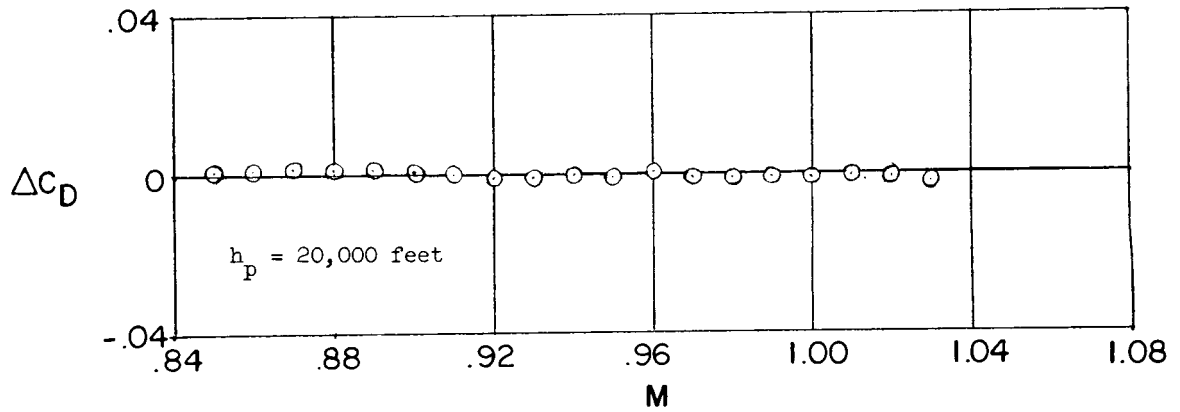
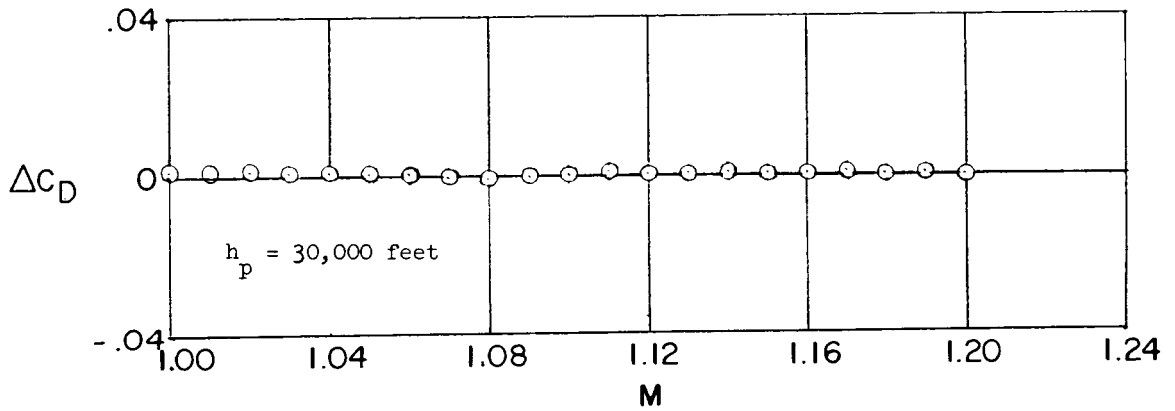


Figure 10.- Comparison of drag-coefficient difference between basic and slats-locked-closed configurations.

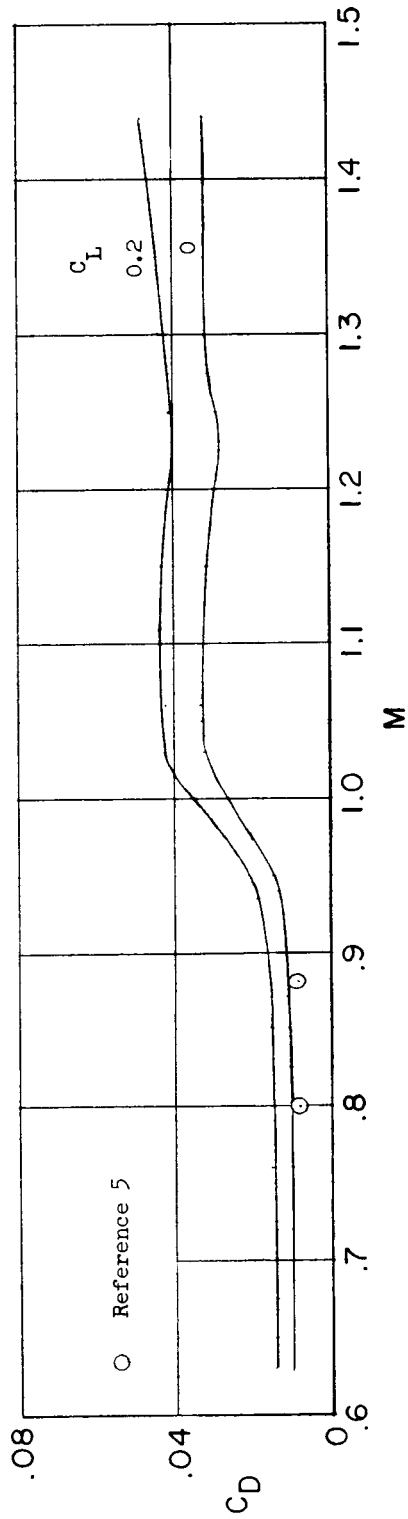


Figure 11.- Variation of drag coefficient with Mach number for lift coefficients of 0 and 0.2.

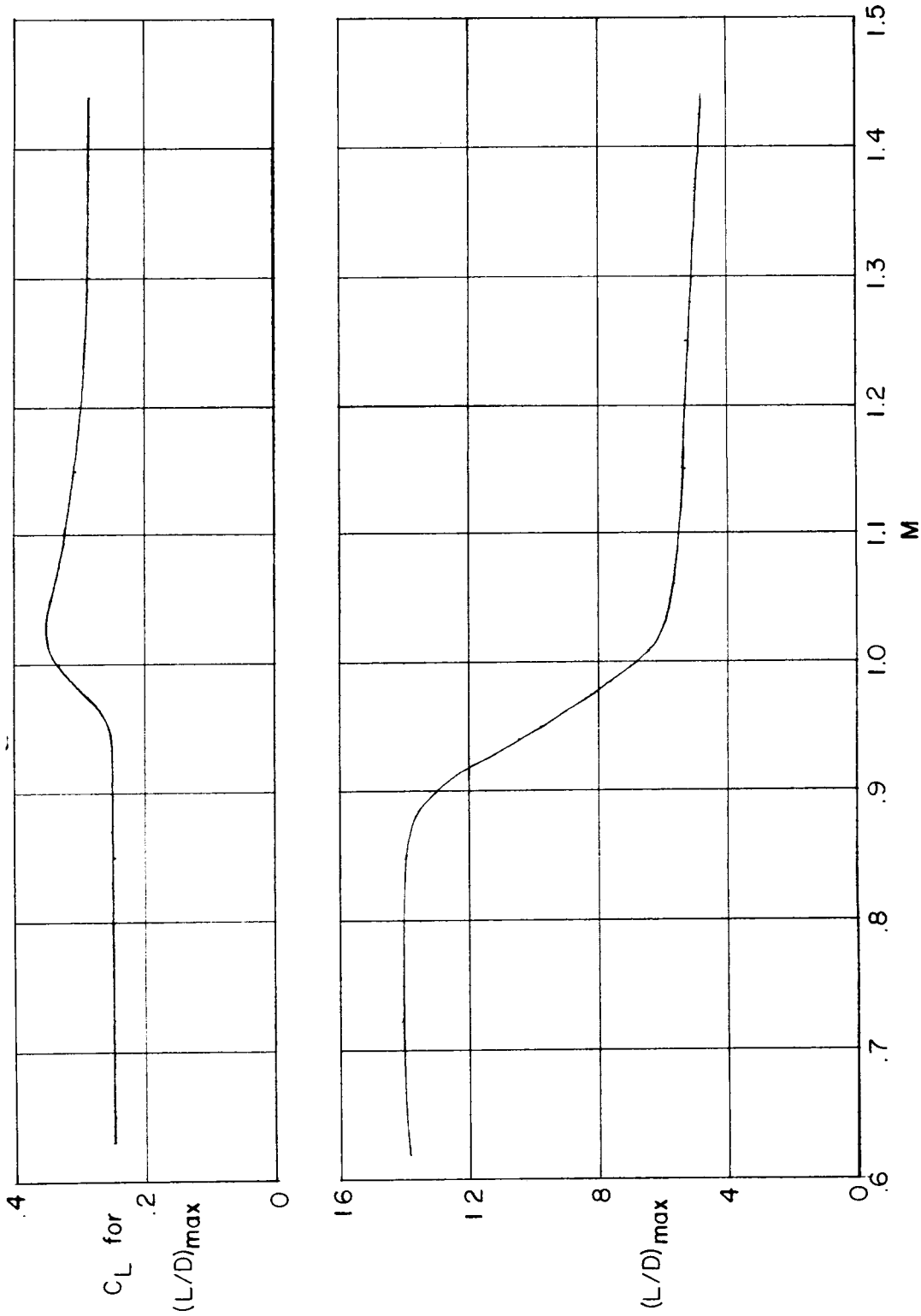


Figure 12.- Maximum lift-drag ratio and lift coefficient for  $(L/D)_{max}$  plotted against Mach number.

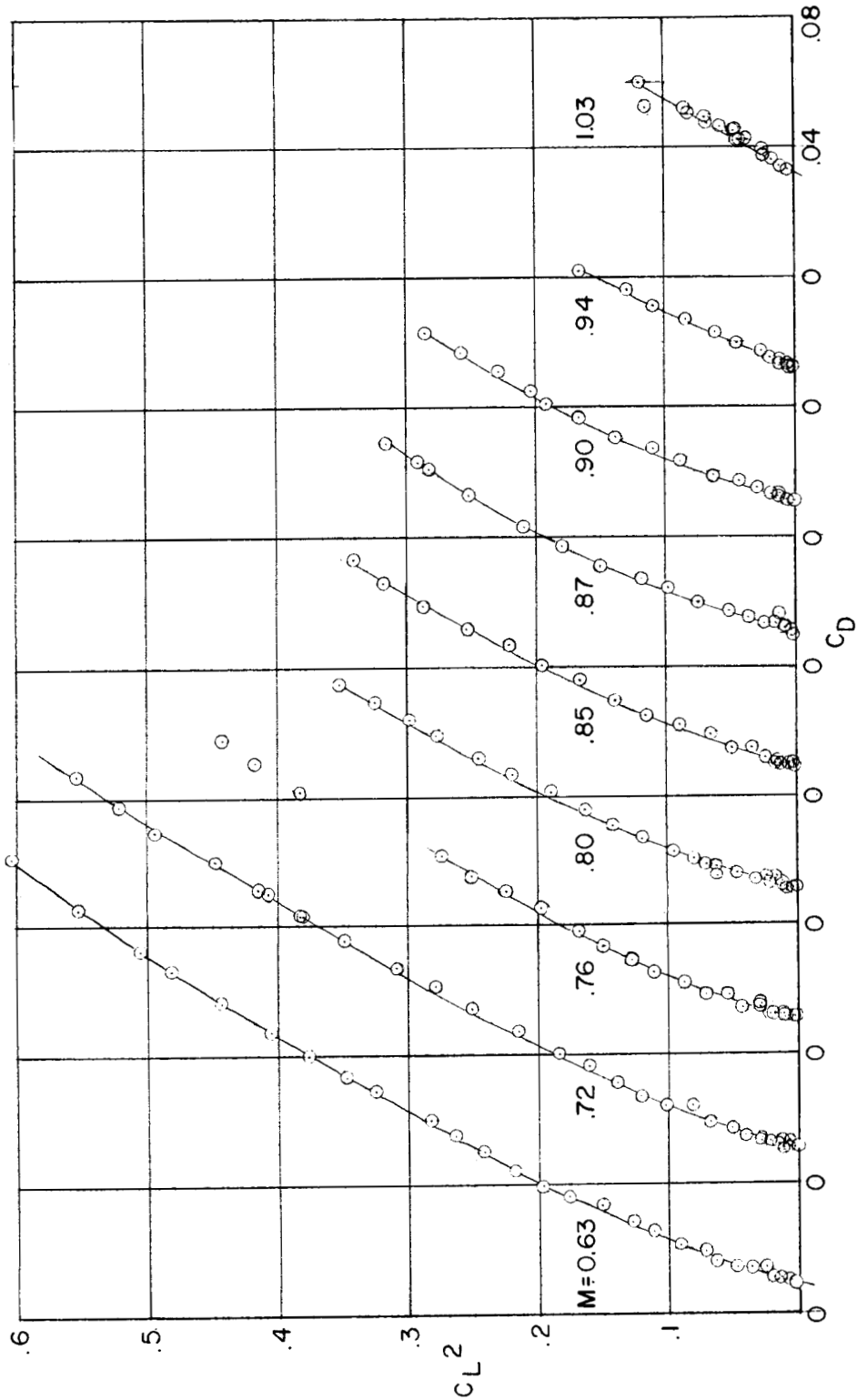


Figure 13.- Square of the lift coefficient plotted against  $C_D$  for several Mach numbers. Basic configuration.

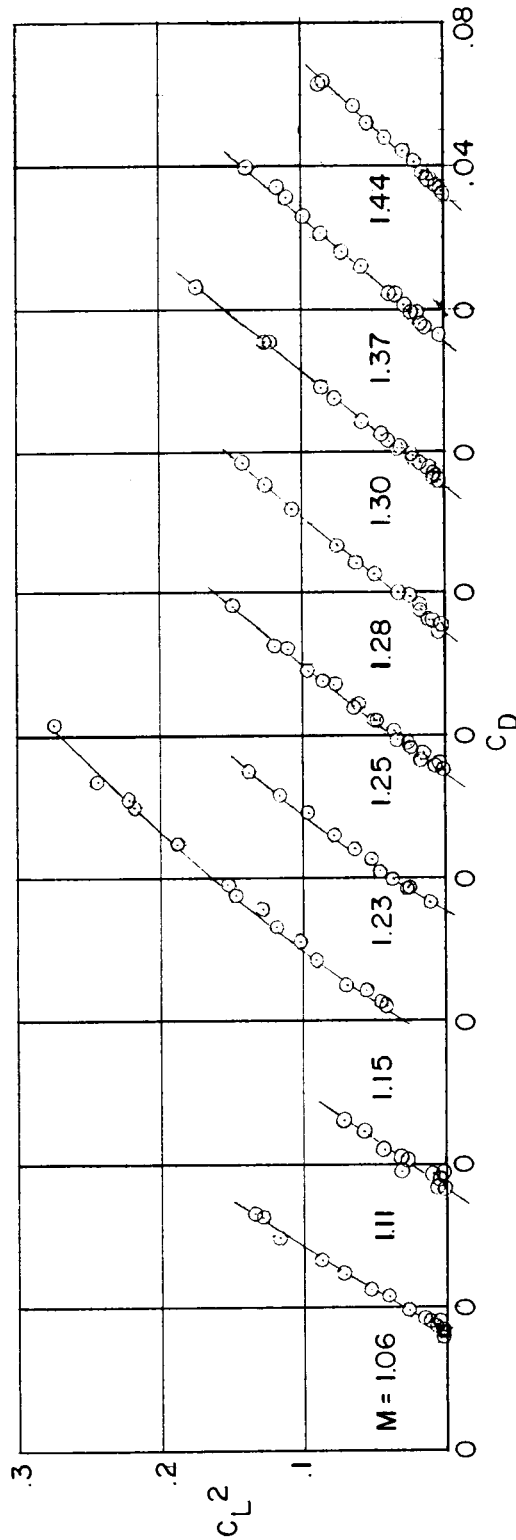


Figure 13.- Concluded.

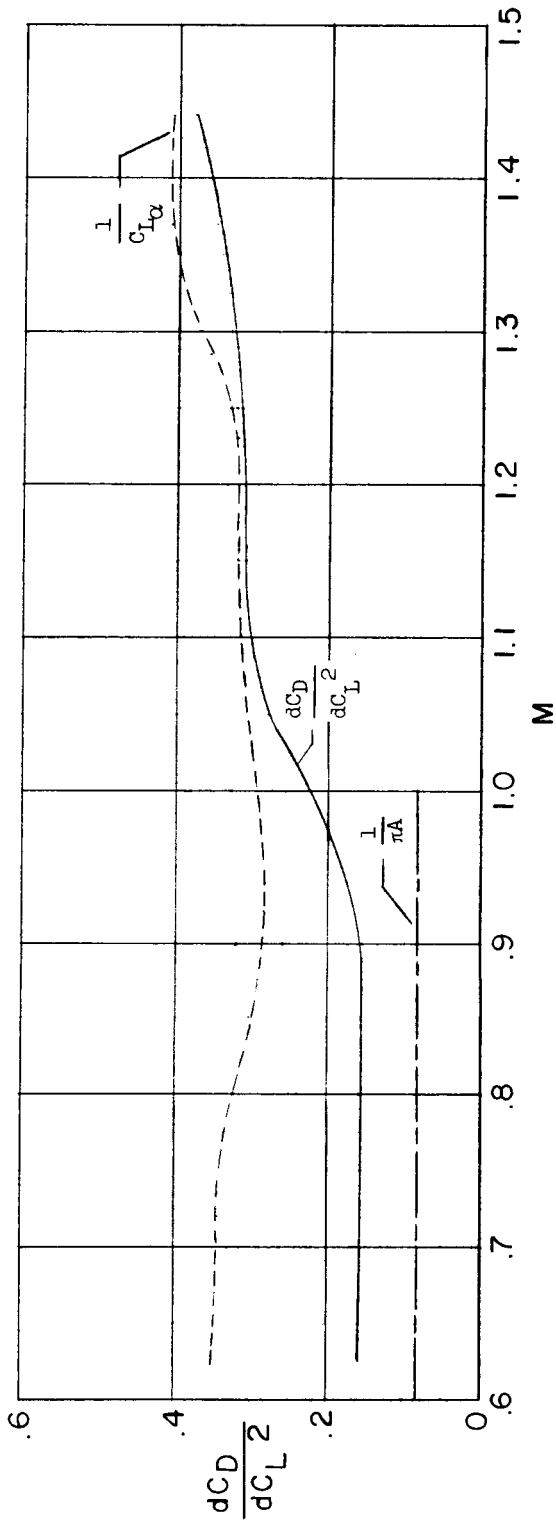


Figure 14.- Variation of drag-due-to-lift factor with Mach number. Low lift.